Langmuir

ARTICLE

pubs.acs.org/Langmuir

Surfactant (Bi)Layers on Gold Nanorods

Sergio Gómez-Graña,[†] Fabien Hubert,[‡] Fabienne Testard,[*,‡] Andrés Guerrero-Martínez,[†] Isabelle Grillo,[§] Luis M. Liz-Marzán,[†] and Olivier Spalla[‡]

[†]Departamento de Quimica Fisica, Universidade de Vigo, 36310 Vigo, Spain

[‡]CEA Saclay, DSM/IRAMIS/SIS2M/LIONS, UMR CEA/CNRS 3299, 91191 Gif sur Yvette, France

[§]Institut Laue-Langevin, BP 156, 38042 Grenoble Cedex 9, France

Supporting Information

ABSTRACT: Gold nanorods in aqueous solution are generally surrounded by surfactants or capping agents. This is crucial for anisotropic growth during synthesis and for their final stability in solution. When CTAB is used, a bilayer has been evidenced from analytical methods even though no direct morphological characterization of the precise thickness and compactness has been reported. The type of surfactant layer is also relevant to understand the marked difference in further self-assembling properties of gold nanorods as experienced using 16-EO_1-16 gemini surfactant instead of CTAB. To obtain a direct measure of the thickness of the surfactant layer on gold nanorods synthesized by the seeded growth method, we coupled TEM, SAXS, and SANS experiments for the two different cases, CTAB and gemini 16-EO_1-16. Despite the strong residual signal from micelles in excess, it can be concluded that the thickness is imposed by the chain length of the surfactant and corresponds to a bilayer with partial interdigitation.

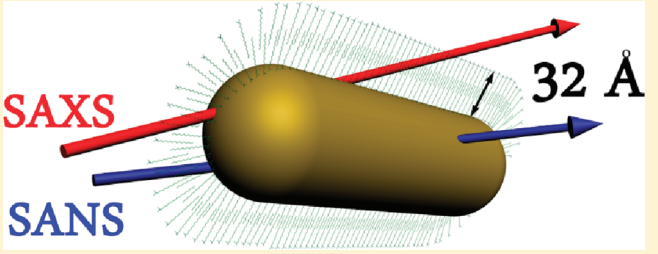

INTRODUCTION

Surfactants are commonly used during the synthesis, stabilization, and crystallization of various types of colloidal nanoparticles including metallic ones. Due to their high versatility, surfactants play a key role in different steps of metal nanoparticles formation such as solubilization of the initial reactants, evolution toward the final nanocrystal shape, and nanoparticle stabilization in different solvents.[1] In the particular case of gold nanorods (GNRs), the surfactant seems to be one of the structure-directing agents inducing anisotropic growth in aqueous media through binding to specific nanocrystal facets.[2] In the seeded growth method in aqueous solution, the most popular synthesis of GNRs,[3,4] a large amount of cetyltrimethylammonium bromide (CTAB) is present, some of it remaining attached to the surfaces at the end of the reaction. When properly dried, these anisotropic nano-objects can self-assemble into 3D superlattices with a parallel orientation with respect to the macroscopic substrate.[5] Moreover, It has been recently shown that when CTAB is replaced by a gemini surfactant,[6] more monodisperse GNRs are obtained with a fascinating capability for 3D self-assembly into standing GNRs superlattices with significantly larger areas.[7] These strong differences between the two cases renew the initial interest to characterize the surface layers of the amphiphilics on GNRs in aqueous solutions. Indeed, the surfactant surface layer is thought to be the source of the colloidal stabilization, and it is known that gemini surfactants have higher surface activity, with higher tendency to form aggregates in solution than their monomeric equivalent.[8,9]

Characterization of the CTAB surfactant layer on GNRs has been reported using TGA, FTIR, and zeta potential.[10,11] The methods used were of analytical nature and thus based on counting the amounts of each species from a relative composition point of view. The extracted values were in good agreement with the presence of a surfactant bilayer on the surface of the GNRs. However, there has been no direct measurement of the morphological characteristics (thickness, density, interdigitation level, and patterning) of such CTAB bilayer. To date, equivalent analytical measurements for gemini surfactant on GNRs are not even available.

Direct imaging of surfactant layers adsorbed on solid macroscopic surfaces could be carried out using atomic force microscopy (AFM). For CTAB on mica substrates, this technique revealed that the nanostructure of the layer varies with time.[12] For a concentration twice the critical micelle concentration (CMC), the layer is initially made of parallel cylindrical micelles of thickness 42 Å with a repetition distance of 70 Å. After 24 h of equilibrium, a flat layer is finally observed. The observed thickness is above that formerly determined by the surface force apparatus (SFA).[13,14] In this technique, a real surface average is obtained in very well-defined geometrical conditions. Moreover, in the SFA technique, the measured thickness could unambiguously be attributed to a repulsive bilayer of CTAB molecules. The

Received: September 2, 2011
Revised: November 10, 2011
Published: December 14, 2011

value found in that case was 33 ± 1 Å. For symmetric gemini surfactants it has been found that the patterning very much depends on the chain length and specific spacers so that longer spacers lead to strong patterning while short ones even lead to flat bilayers on mica.[15] All these experiments have the advantage to be performed in situ with the presence of solvent. Their main drawback is the macroscopic dimension of the surfaces, even if AFM probes only a very small part of it.

An excellent way to probe in situ the structure of nanoobjects is small angle scattering of either X-rays or neutrons (denoted as SAXS and SANS, respectively).[16,17] These techniques are particularly sensitive to the shape of the objects in a size ranging from 1 nm to a few hundreds of nanometers.[18] When the objects are made of two different materials, as it is the case in GNRs stabilized by surfactants, neutrons further offer the capability to change the relative weight of each material in the scattering signal. This contrast variation technique is very popular in biology and soft matter where X-rays can hardly distinguish between functional groups.[19] For aqueous solutions, this technique has been used to characterize the thickness of the surfactant bilayer stabilizing aqueous magnetic fluids[20,21] or to measure the structure of nonionic surfactant layers adsorbed on spherical monodisperse silica.[22,23] In this last example, the average thickness together with the inner structure of the surfactant layer was accessible showing that a silica bead was decorated with micelles whose shape depends on the silica core size. Concerning gold nanoparticles dispersed in aqueous phase, few examples can be found about the SANS characterization of the surrounding surfactant layer.[24,25]

In this work, small angle scattering was used to gain a better characterization of the surfactant layer remaining on GNRs after seeded growth synthesis for both the classical CTAB and a gemini surfactant counterpart and to reveal the possible differences between them. This was a challenging task due to the typically very low concentration of nano-objects in solution, their potential nanoparticle polydispersity in size and shape, together with the inherent presence of free micelles in solution. Therefore, to obtain firmly experimentally grounded conclusions we coupled both SAXS, to determine the polydispersity, and SANS, to obtain the morphological characteristics of the surfactant layer.

MATERIALS AND METHODS

Synthesis and Sample Preparation for Scattering Analysis. *Gemini Surfactant.* (Oligooxa)alkanediyl-α,ω-bis(dimethylhexadecylammonium) bromide surfactant (16-EO$_1$-16) was synthesized according to procedures described in the literature.[26]

Seed Solution. CTAB solution (4.7 mL, 0.1M) was mixed with 25 μL of 0.05 M $HAuCl_4$. A 300 μL amount of sodium borohydride (0.01 M) was added quickly and with vigorous stirring. The resulting solution of CTAB-stabilized gold seeds (2−3 nm) was kept at 30 °C.

GNRs Synthesis in CTAB. GNRs were prepared by seeded growth.[4,27] The seeds were grown in the presence of CTAB (0.1 M), $HAuCl_4$ (0.5 mM), $AgNO_3$ (0.06 mM), and ascorbic acid (0.75 mM) as a mild reducing agent. The growth solution was kept at 30 °C for 2 h in a thermostated bath. GNRs were purified by centrifugation (3500 rpm, r = 4.5 cm, 20 min), significantly decreasing the content of spheres obtained after synthesis.

GNRs Synthesis in Gemini Surfactant. Analogously to the previous synthesis, GNRs were prepared by seeded growth at 30 °C through reduction of $HAuCl_4$ with ascorbic acid on CTAB-stabilized gold seeds in the presence of 16-EO$_1$-16 (0.05 M), HCl (pH 2−3), and $AgNO_3$ (0.12 mM).[7] After synthesis no further purification of GNRs was performed.

Sample Preparation for Scattering Analysis (Purification and Solvent Exchange versus Stability of GNRs). Use of scattering techniques requires obtaining stable dispersions of GNRs with a minimum of additional components in solution (gold nanoparticles with different morphologies and surfactant micelles). As a first stage, the best possible separation of spherical particles from the GNRs is required. For CTAB, one centrifugation step was used to minimize the spheres content as described above. Regarding 16-EO$_1$-16, the different attempts of shape purification were not effective and samples had to be used as such. A second requirement is to reduce the excess of free surfactant (CTAB or 16-EO$_1$-16) derived from GNRs synthesis. However, the surfactant molecules in the layer around the GNRs are in dynamic equilibrium with free surfactant molecules in solution. It is known that aggregation of GNRs can be induced when the purification process is pushed too far, usually decreasing the concentration of surfactant below the CMC.[28] In the present case, this problem also occurred during the solvent exchange step and attempts to replace the supernatant after centrifugation by pure water induced aggregation in a few minutes. As a consequence, the following protocol was followed: after synthesis and one centrifugation step when necessary (as described above), the GNRs solutions were centrifuged three times (8000 rpm, r = 4.5 cm, 40 min) to remove excess reactants. The final concentration of surfactants was kept at the CMC of CTAB (1 mM) and 16-EO$_1$-16 (0.5 mM) to avoid undesired agglomeration of particles. Analogously for SANS experiments, the procedure was repeated three times more using solutions of pure D_2O or a mixture (H_2O/D_2O) at the contrast matching condition with surfactants at their respective CMCs. During all these sample preparations the absorbance at 400 nm was used to quantify the total concentration of gold atoms in solution,[29] and the stability of the GNRs was checked by following both the transversal and the longitudinal plasmon bands in the corresponding extinction spectra. Two gold concentrations (2.5 and 6 mM) were chosen for this study.

Size and Shape Characterization. After the synthesis and washing steps, TEM samples were prepared from the obtained solutions by drying one droplet on a carbon-coated copper TEM grid. The grids were analyzed in a JEOL JEM 1010 TEM operating at an acceleration voltage of 100 kV. Analysis was performed on 750 particles to describe the distribution in size and shape of the gold nanoparticles.

The SAXS experiments were performed in a home-built camera at the LIONS laboratory. The SAXS camera is equipped with a copper rotating anode, collimating optics, and a MAR 2D detector. Samples were analyzed in a borosilicate capillary with a 1.5 mm path length. After radial averaging, the intensity was calibrated using the classical procedures.

The SANS experiments were performed at the ILL on D22 beamline. Three configurations were used at λ = 0. 8 nm to ensure a large final q range from 2.31 × 10^{-3} to 5.37 × 10^{-1} Å^{-1}. Typical acquisitions in 1 mm path length cells were 4000−6000 s for the low q range, 2200−3600s for the medium q range, and 600−900s for the high q range depending on the composition of the solvent (D_2O or contrast match). Absolute intensities were obtained after radial averaging using the classical procedure developed at ILL.[30]

Analysis of the Scattering Diagrams. The SAXS and SANS diagrams were fitted using the particular distribution of cylinders as revealed by the TEM images.[31] Indeed, the distribution of the width and length around their mean (R_0, L_0) is not decoupled as usually assumed.[32] Using a representation of diameters versus lengths (L, D) of the individual nanoparticles it was unraveled that the cloud of nanoparticles is distributed along two major axis (u, v), rotated with an angle θ as compared to (L, D)

$$\begin{aligned} L &= L_0 + u\cos(\theta) - v\sin(\theta) \\ R &= R_0 + u\sin(\theta) + v\cos(\theta) \end{aligned} \quad (1)$$

In the present cases the distribution in size and shape was experimentally obtained from TEM analysis. The distributions were fitted with a Gaussian shape in u and v (eq 2)

$$f(u,v) = \frac{1}{\sqrt{2\pi}\sigma_v \times \sqrt{2\pi}\sigma_u} e^{-v^2/2\sigma_v^2} \times e^{-u^2/2\sigma_u^2} \quad (2)$$

dx.doi.org/10.1021/la203451p |Langmuir 2012, 28, 1453–1459

Table 1. Parameters Issued from TEM GNRs Distribution (R_0, L_0, σ_u, σ_v, θ) with the (L, D) Representation and Used To Calculate the Theoretical SAXS Intensity (fitted values, when done, instead of TEM measured ones are in italic)[a]

surfactant (concentration)	[Au], mM (UV)	R_0, Å	L_0, Å	σ_u (for TEM)	σ_v	θ	σ_v (SANS)	t, Å
CTAB (6 mM)	5.2	56.5	359	*20* (10)	8	0.076	8	34
16-EO_1-16 (6 mM)	5.6	53.0	260	*20* (10)	6	0.149	12	30
CTAB (2.5 mM)	2.1	54.5	342	20	8	0.101	10	34
16-EO_1-16 (2.5 mM)	2.5	61.5	313	8	10	0.131	10	34

[a] These parameters are used to fit SANS patterns with the thickness t of the organic layer as the single variable.

In summary, the experimental TEM cloud is described by five parameters R_0, L_0, σ_u, σ_v, and θ.

Using these distributions, the SAXS and SANS scattering intensities can be calculated. Regarding the SAXS diagrams, the contrast in scattering length density (proportional to electron density) is very strong between the gold core and water,[18,33] well above the contrast between water and the surfactant layer.[18,33] Accordingly, two levels of scattering length density (SLD) are enough to describe the system. Thus, the fits were performed using a summation of the intensities over this (u, v) type of distribution (eq 3)

$$I(q) = N(\Delta\rho)^2 \iint f(u,v)V^2 P_{cyl}(q,R,L)\mathrm{d}u\ \mathrm{d}v \qquad (3)$$

where N (cm^{-3}) is the number density of objects, $\Delta\rho$ (1.21×10^{12} cm^{-2}) is the scattering length density contrast between gold and water,[33] $f(u,v)$ is the normalized distribution over u and v, and V and P_{cyl} are the volume and form factor of a cylinder of dimension L and R, respectively.

$$P_{cyl}(q,R,L) = \int_0^{\pi/2} A_{cyl}^2(q,R,L,\varphi)\sin(\varphi)\mathrm{d}\varphi \quad \text{with}$$

$$A_{cyl}(q,R,L,\varphi) = \left\{ \frac{2J_1(qR\sin\varphi)}{qR\sin\varphi} \frac{\sin((qL/2)\cos\varphi)}{(qL/2)\cos\varphi} \right\} \qquad (4)$$

In most cases, direct use of the distribution parameters deduced from TEM yields perfectly satisfying fit of the SAXS diagrams. However, in some occasions, slight adjustment were required. All size parameters obtained by TEM and SAXS analysis are listed in Table 1.

For the SANS experiments, three levels of scattering length density are needed. The SLD were calculated using the NIST CNR scattering length density calculator.[34] One gets 6.38×10^{-10} cm^{-2} for the D_2O solvent, -0.3×10^{-10} cm^{-2} for the alkyl chain layer, and 4.51×10^{-10} cm^{-2} for the gold core. The latter can also be matched by a solvent mixture of 75%$_v$ D_2O and 25%$_v$ H_2O.[18,30] The SLD profile takes into account the surfactant polar head layer but not its solvation due to its small size compared to the core radius and the alkyl chain thickness. Accordingly, no single contrast is dominating the two others, and three levels of scattering length density are mandatory to properly describe the system. For D_2O solvent or D_2O/H_2O mixture, a model for core−shell nanorods was used to calculate the intensity scattered by nanoparticles surrounded by a surfactant layer. For core−shell GNRs with a constant layer thickness t and a polydispersity in u and v the scattering intensity is given by (eq 5)

$$I(q) = N \int \int \int_0^{\pi/2} f(u,v)A^2 \sin\varphi\ \mathrm{d}\varphi\ \mathrm{d}u\ \mathrm{d}v \qquad (5)$$

with

$$A = (\rho_3 - \rho_2)\times V(R + t, L + 2t) \times A_{cyl}(q, R + t, L + 2t, \varphi) + (\rho_2 - \rho_1) \times V(R,L) \times A_{cyl}(q,R,L,\varphi) \qquad (6)$$

The resolution of the instrument has been taken into account in the final determination of the scattered intensity $I(q)$ using the classical procedure

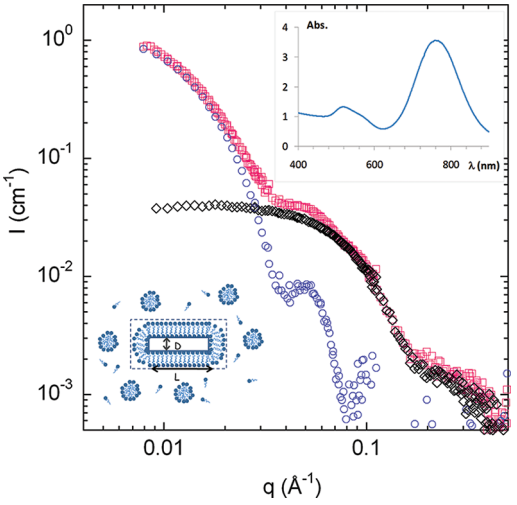

Figure 1. SANS pattern of (□) GNRs solution in D_2O ([Au] = 2.5 mM, [CTAB] ≈ CMC) and (◇) CTAB micelles ([CTAB] ≈ CMC). (○) SANS pattern of GNRs solution after subtraction of the signal from residual CTAB micelles. (Insets) UV−vis spectra of the gold nanorods solution (top right) and schematic view of GNRs in equilibrium with micelles and monomers (bottom left) are shown.

described in ref 17 . On the basis of the $f(u,v)$ determination by TEM or slight adjustments of it to recover the SAXS diagram the calculated SANS diagrams were fitted to the experimental ones using only the thickness t as a parameter (see Table 1). The concentration of GNRs is imposed by the value found by SAXS fitting. Using the same set of parameters to reproduce TEM, SAXS, and SANS in D_2O and SANS at the contrast match is a strong validation to characterize the GNRs and particularly the surfactant layer stabilizing them.

RESULTS AND DISCUSSION

GNRs in Equilibrium with Excess Micelles. After purification and solvent exchange of GNRs, the SANS patterns of a D_2O solution of GNRs ([Au] = 2.5 mM) stabilized by CTAB in equilibrium with an excess of CTAB (∼CMC) is shown in Figure 1. The signal coming from the CTAB micelles in D_2O in the absence of nanoparticles was added on the same graph for comparison. It clearly appears that in the GNRs sample scattering intensity the residual signal coming from the free micelles cannot be neglected as compared to the total scattered intensity, especially at large q. Therefore, the intensity from these micelles must be subtracted to correctly identify the signal from the GNRs and their surrounding surfactant shell. The experimental SANS signal from residual CTAB micelles ([CTAB] = CMC) was subtracted from the SANS signal from GNRs solution stabilized by CTAB (as shown in Figure 1). Subtraction does not affect the positions of the minima but enhances the amplitude of the

dx.doi.org/10.1021/la203451p |*Langmuir* 2012, 28, 1453–1459

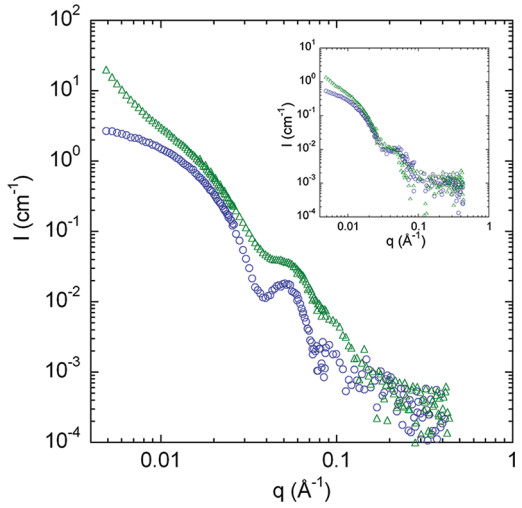

Figure 2. SANS patterns of GNRs solution in D_2O ([Au] = 6 mM in D_2O), stabilized with 16-EO_1-16 (Δ) or CTAB (○). (Inset) SANS patterns of GNRs solution ([Au] = 2.5 mM) at the contrast match (H_2O/D_2O, 25/75) stabilized by 16-EO_1-16 (Δ) or CTAB (○).

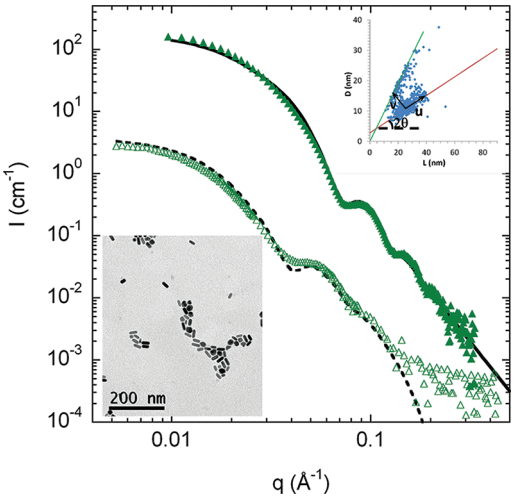

Figure 3. SAXS and SANS patterns of GNRs stabilized by 16-EO_1-16 ([Au] = 6 mM and [16-EO_1-16] = 0.5 mM): (▲) SAXS; (Δ) SANS for D_2O solution; lines correspond to the theoretical curves obtained with the parameters given in Table 1. (Insets) (right) Experimental TEM distribution used to calculate the SAXS and the SANS intensity for GNRs covered by an organic layer with a thickness of 30 Å; (left) TEM image of the sample in D_2O.

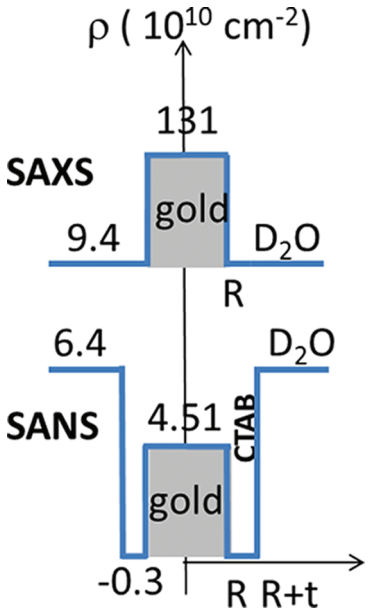

Figure 4. SAXS and SANS scattering length densities for a GNR stabilized by CTAB layers.

oscillation. This scattered intensity is quite low (below 10^{-2} cm^{-1}) in the interesting q range (0.03−0.1 $Å^{-1}$) for the selected gold concentration ([Au] = 2.5 mM). This value corresponds to a GNR solid volume fraction equal to 2.6×10^{-5}, a very low value 3 orders of magnitude lower than the silica solid volume fraction used in the recent study on surfactant-coated silica.[22,23] Moreover, considering an average radius of 56 Å for the gold core of GNRs, the volume fraction of adsorbed bilayer (assuming a thickness of 34 Å) would be 4×10^{-5}, leading to a surfactant concentration 0.1 times the CMC for CTAB. Accordingly, the concentration of gold was increased to 6 mM to raise the signal-to-noise ratio by a factor of two. Above 6 mM, the aggregation between GNRs was too important to allow correct measurements. The signal from residual micelles remains a strong limitation to characterize the organic shell around GNRs because the surfactant layer is not static as described in the literature for CTAB,[35] and thus, it is not possible to eliminate completely the unbound CTAB without aggregation of the GNRs. Thus, the method used here ensures the stability of the GNRs with a control on the concentration of the excess surfactant. However, as shown in Figure 1 subtraction is not reliable beyond $q = 0.1$ $Å^{-1}$.

The general behavior is very similar for the GNRs stabilized with the gemini (16-EO_1-16) surfactant, where an excess of surfactant was also necessary to ensure stability. However, for 16-EO_1-16 the tendency toward aggregation was found to be higher as shown in Figure 2, due to the high amphiphilic character that gemini surfactants display in water.[36,37] At 6 mM, an increase of the intensity in the low q-range region was observed in the SANS patterns of GNRs stabilized by 16-EO_1-16 in D_2O, contrary to the CTAB case. This behavior is in agreement with the specific self-assembly properties of GNRs stabilized with gemini surfactants recently evidenced.[7] For further analysis and shape fitting, the q^{-4} regime due to the envelope of the self-assembled GNRs was subtracted following a classical procedure.[38]

Characterization of the Bilayer by Coupling SAXS and SANS. As an initial statement about the coupling of SAXS and SANS results, these two patterns for the GNRs stabilized by 16-EO_1-16 in D_2O ([Au] = 6 mM and [16-EO_1-16] = 0.5 mM) are compared in Figure 3. In the SANS pattern, one observes a shift of the oscillation toward a lower q value, an indication that neutrons are seeing thicker objects than X-rays. The marked difference in the q dependence of the two signals is direct proof of a system with more than two levels of scattering. These levels correspond to the gold core, the surfactant layer, and the solvent. For SAXS patterns, as already mentioned, the X-rays are interacting with the electrons of the material. As a consequence, the surfactant and water having close values of electronic densities as compared to the gold core, the surfactant shell does not show a strong signature in the SAXS diagram. On the contrary, the large difference of scattering lengths for neutrons between H and D can be exploited in SANS to characterize the surfactant layer.

dx.doi.org/10.1021/la203451p |*Langmuir* 2012, 28, 1453–1459

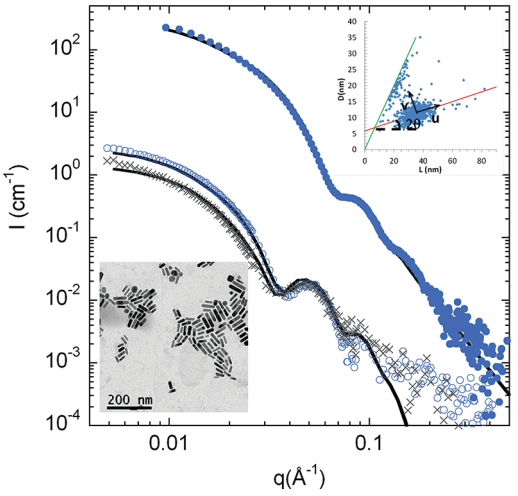

Figure 5. SAXS and SANS patterns of GNRs stabilized by CTAB ([Au] = 6 mM and [CTAB] = 1 mM): (●) SAXS; (○) SANS for D_2O solution; (×) SANS for the same solution at the contrast match of gold (D_2O/H_2O (75/25)); lines correspond to the theoretical curves obtained with the parameters given in Table 1. (Insets) (right) Experimental TEM distribution used to calculate the SAXS and SANS intensity for gold nanorods covered by an organic layer with a thickness of 34 Å; (left) TEM image of the sample in D_2O.

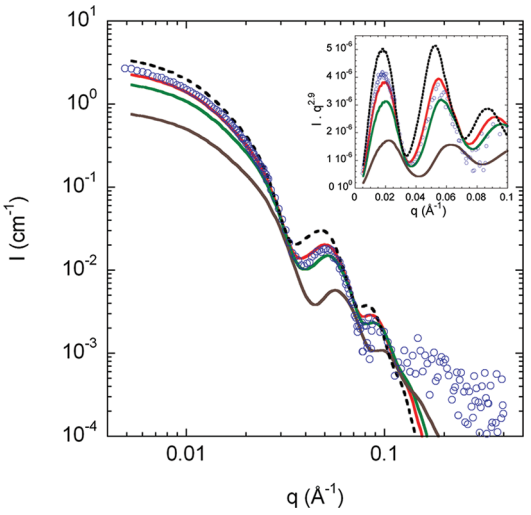

Figure 6. Effect of the thickness t on the SANS scattered intensity for similar (R_0,L_0,σ_w,σ_v,θ_0) and constant number of gold nanoparticles for GNRs stabilized by CTAB ([Au] = 6 mM, [CTAB] = CMC): t = 40 Å (black dotted line), t = 34 Å (red line), t = 30 Å (green line), t = 20 Å (brown line)); the SLD of the organic layer is equal to -0.3×10^{10} cm^{-2}. (Inset) $I \times q^{2.9}$ versus q representation.

The profiles of scattering length density for the GNRs stabilized by surfactant in D_2O are given in Figure 4. The gold core nanoparticles can even be matched by a D_2O/H_2O mixture. Similar results were obtained for GNRs stabilized by CTAB in D_2O ([Au] = 6 mM and [CTAB] = 1 mM) (Figure 5). Figure SI-1 (Supporting Information) shows the same results for lower gold concentration ([Au] = 2.5 mM) for the two surfactants CTAB and 16-EO$_1$-16.

The analysis can be pushed beyond the initial conclusion that a layer different from pure gold is present on the surface of the GNRs. A quantitative fitting of the scattering data was performed using eqs 1−6. First, the SAXS theoretical intensity was calculated with the parameters issued from the TEM nanoparticle distribution in (L,D) representation. It matches the experimental SAXS patterns as shown in Figure 3 for GNRs stabilized by 16-EO$_1$-16 and in Figure 5 for GNRs stabilized by CTAB. It is remarkable that the obtained nanoparticles were not described by a Gaussian distribution in R and L but in u and v defined by the anisotropic branch in the (L,D) representation (shown in the inset of Figure 3 for 16-EO$_1$-16 and Figure 5 for CTAB). The parameters are summarized in Table 1, and one can note that 16-EO$_1$-16 leads to shorter GNRs than CTAB, with a similar diameter and polydispersity in v. In a second stage, the same (L,D) distributions were used to calculate the SANS intensity using the thickness t and scattering length density ρ_2 of the surfactant layer to adjust the calculated curves on the experimental ones. The scattering length density of an alkyl chain is usually taken around -0.3×10^{10} cm^{-2}.[18,39] The SAXS pattern and two SANS patterns (D_2O and the contrast match condition) could be fitted using a common set of morphological parameters. They are shown in Figure 5 for the GNRs stabilized by CTAB (and in Figure SI_2, Supporting Information for GNRs stabilized by 16-EO1−16 for [Au] = 2.5 mM). The fit of three different curves with a common set of parameters strongly supports the morphological conclusions that can be extracted. The best fits were obtained for a thickness of 34 Å. This value is in agreement with the study of Kékicheff et al.,[13] in which a 33 Å thickness for a CTAB bilayer on mica immersed in aqueous CTAB micelle solution has been reported using the surface force apparatus.[14] This is also in agreement with the results from Sau et al.[11] by TEM on dried GNRs stabilized by CTAB, where the smallest interparticle distance was found to be 34 Å, suggesting that only two layers of CTAB are present between the obtained dried GNRs. The fit using a homogeneous layer of surfactant overlaps the experimental points up to q = 0.1 Å^{-1} and deviates slightly above this value. However, as already mentioned, the subtracted data are very noisy beyond this q value due to the presence of the micelle signal in the raw data and we do not consider this deviation as reliable. Accordingly, it is not possible to measure the potential inner nanostructure of the layer as in the case of silica.[22]

Similar results were obtained for GNRs stabilized by 16-EO$_1$-16 (Figure 3 and Figure SI_2, Supporting Information) with a thickness of 30−34 Å for the two different gold concentrations. One can note that the agreement with a flat bilayer goes in that case up to q = 0.15 Å^{-1} due to a lower CMC contribution.

We stress that the calculated scattering intensity is very sensitive to the thickness t as demonstrated in Figure 6 (CTAB case) where four different thicknesses were tested (40, 34, 30, and 20 Å) for a given concentration of gold nanoparticles using the scattering length density (ρ_2) of CTAB for the organic layer. The value of 34 Å yields the best fit, and even if 30 Å is within the experimental accuracy, the two other extreme values (20 and 40 Å) can be discarded (for both the position of the minima and the values of the intensity). Definitely a monolayer with a small fraction of extra charge (a start of double layer), mandatory to ensure colloidal stability, can be eliminated. Regarding the scattering length density of the organic layer ρ_2 the model shows that it is not possible to recover the experimental intensity by increasing ρ_2 above 1.0×10^{10} cm^{-2} (i.e., increasing the hydration of the organic layer above 20%). As shown in the Supporting Information, for a given concentration in GNRs and a constant amount of adsorbed surfactant a larger thickness (corresponding to a

dx.doi.org/10.1021/la203451p |Langmuir 2012, 28, 1453–1459

larger ρ_2) is incompatible with the experimental scattered intensity in absolute units. Hence, applied to the present cases, the sensitivity analysis gives the following. For both CTAB and 16-EO_1-16 surfactants, the fitting is sensitive to the thickness of the layer and we can definitely conclude that the thickness is neither 40 nor 20 Å, the best value laying in the window 30−34 Å.

The comparable values for 16-EO1-16 and CTAB surfactants layers reflect the equal length of their alkyl chains. Indeed, this surfactant feature imposes the overall layer thickness, more than the hydrophilic headgroup type does. However, in both cases, the measured layer thickness is less than a full compact double layer of surfactant. Indeed, a completely extended alkyl chain would be around 20 Å leading to a bilayer of 40 Å. Taking into account that these two values were firmly discarded, we propose a model of surfactant−nanoparticle interaction in which CTAB or 16-EO_1-16 builds up a bilayer by interdigitation of the alkyl tails by strong hydrophobic interactions. The obtained bilayer stabilizes the GNRs in solution. This is a first demonstration that the bilayer is fully expanded at the surface of the GNRs, since the dimension of the surfactant layer was not accessible with the previous techniques used. Finally, beyond the overall thickness of the surfactant layer it is also found that the type of surfactant head strongly influences the stability, as shown by the enhanced tendency of the 16-EO_1-16 stabilizing layer to induce attractive interactions between the GNRs when the concentration is increased.

CONCLUSIONS

Complementary measurements of SAXS and SANS have allowed us to extract a fine picture of the structure of GNRs stabilized by a surfactant layer. SAXS was used to characterize the gold cores. The unique feature of neutrons with contrast variation combined with the very high flux of the D22 spectrometer have permitted one to extract the layer signal from that of free micelles and to determine the thickness of the CTAB and 16-EO1-16 surfactant layers. A bilayer thickness of 32 ± 2 Å with an almost nominative alkyl chain density (80−100%) was observed for the two cases within the experimental accuracy. These results confirm the presence of a surfactant bilayer on the surface of GNRs, a result which was widely accepted but opens the question of a potential interdigitation of the alkyl chain as the obtained thickness is smaller than the extended alkyl chain length. However, some questions remain open. No internal patterning of the bilayer could be detected due to the overall weakness of the signal arising from the intrinsic low concentration of this type of GNRs suspension and a strong contribution from free micelles. More details could have been obtained by increasing the GNRs concentration by at least 1 order of magnitude; unfortunately, the corresponding suspensions were not sufficiently stable with time. Accordingly, measurement of a different amount of adsorption on the ends of the nanorods as compared to the lateral facets, which is often invoked as the source of the anisotropic growth and chemical reactivity of GNRs, is still to be demonstrated by direct structural techniques.

ASSOCIATED CONTENT

Supporting Information. SAXS and SANS patterns of GNRs stabilized by 16-EO1-16 or CTAB in D_2O for a lower gold concentration: [Au] = 2.5 mM; experimental and theoretical SAXS and SANS patterns of GNRs stabilized by 16-EO1-16 in D_2O and at the contrast match of gold ([Au] = 2.5 mM); influence of the scattering length density (ρ_2) on the scattered intensity from GNRs stabilized by surfactant layer of thickness "t". This material is available free of charge via the Internet at http://pubs.acs.org.

AUTHOR INFORMATION

Corresponding Author
*E-mail: fabienne.testard@cea.fr.

ACKNOWLEDGMENT

This work has been funded by the Spanish Ministerio de Ciencia e Innovación (MAT2010-15374 and CTQ2010-18576) by the EU (NANODIRECT, grant number CP-FP 213948-2). A.G.M. acknowledges the Isidro Parga Pondal Program (Xunta de Galicia, Spain). We thank ILL (Institut Laue-Langevin) for the allocated beam-time and LLB (Laboratoire Léon Brillouin) for preliminary experiences. Fabrice Cousin is thanked for his help at the starting of SANS experiments.

REFERENCES

(1) Xia, Y.; Xiong, Y.; Lim, B.; Skrabalak, S. E. *Angew. Chem., Int. Ed.* **2009**, *48*, 60–103.
(2) Murphy, C. J.; Thompson, L. B.; Alkilany, A. M.; Sisco, P. N.; Boulos, S. P.; Sivapalan, S. T.; Yang, J. A.; Chernak, D. J.; Huang, J. *J. Phys. Chem. Lett.* **2010**, *1*, 2867–2875.
(3) Jana, N. R.; Gearheart, L.; Murphy, C. J. *Chem. Mater.* **2001**, *13*, 2313–2322.
(4) Nikoobakht, B.; El-Sayed, M. A. *Chem. Mater.* **2003**, *15*, 1957–1962.
(5) Ming, T.; Kou, X.; Chen, H.; Wang, T.; Tam, H.-L.; Cheah, K.-W.; Chen, J.-Y.; Wang, J. *Angew. Chem., Int. Ed.* **2008**, *47*, 9685–9690.
(6) Zana, R.; Talmon, Y. *Nature* **1993**, *262*, 228–230.
(7) Guerrero-Martínez, A.; Pérez-juste, J.; Carbo-Argibay, E.; Tardajos, G.; Liz-Marzán, L. M. *Angew. Chem., Int. Ed.* **2009**, *48*, 9484–9488.
(8) Borse, M.; Sharma, V.; Aswal, V. K.; Goyal, P. S.; Devi, S. *J. Colloid Interface Sci.* **2005**, *284*, 282–288.
(9) Zana, R. *J. Colloid Interface Sci.* **2002**, *248*, 203–220.
(10) Nikoobakht, B.; El-Sayed, M. A. *Langmuir* **2001**, *17*, 6368–6374.
(11) Sau, T. K.; Murphy, C. J. *Langmuir* **2005**, *21*, 2923–2929.
(12) Ducker, W. A.; Wanless, E. J. *Langmuir* **1999**, *15*, 160–168.
(13) Kékicheff, P.; Christenson, H. K.; Ninham, B. W. *Colloids Surf.* **1989**, *40*, 31–41.
(14) Richetti, P.; Kékicheff, P. *Phys. Rev. Lett.* **1992**, *68*, 1951–1954.
(15) Manne, S.; Schäffer, T. E.; Huo, Q.; Hansma, P. K.; Morse, D. E.; Stucky, G. D.; Aksay, I. A. *Langmuir* **1997**, *13*, 6382–6387.
(16) Narayanan, T. In Applications of Synchrotron Light to Scattering and Diffraction in Materials and Life Sciences. *Lecture Notes Phys.*, Berlin: springer, 2009; Vol. 776, Chapter synchrotron, small-Angle X-ray scattering studies of colloidal suspensions, pp 133−156.
(17) Grillo, I. In *Soft Matter characterization*. Springer-Verlag: Berlin, Heidelberg, 2008; Chapter 13 (Small-angle neutrons scattering and applications in soft condensed matter), pp 705−782.
(18) Lindner, P.; Zemb, T. *Neutrons, X-rays and light: Scattering Methods Applied to soft Condensed Matter*; Elsevier: North-Holland Delta Series, 2002.
(19) Schurtenberger, P. In *Neutron, X-rays and light: Scattering Methods Applied to soft Condensed Matter*; Elsevier: North-Holland Delta Series, 2002; Chapter 7 (Contrast and contrast variation in neutron, x-ray and light scatering), p 145.
(20) Shen, L.; Laibinis, E.; Hatton, T. A. *J. Magn. Magn. Mater.* **1999**, *194*, 37–44.
(21) Patel, R.; Upadhyay, R. V.; Aswal, V. K.; Joshi, J. V.; Goyal, P. S. *J. Magn. Magn. Mater.* **2011**, *323*, 849–856.

(22) Lugo, D. M.; Oberdisse, J.; Karg, M.; Schweins, R.; Findenegg, G. H. *Soft Matter* **2009**, *5*, 2928–2936.
(23) Lugo, D. M.; Oberdisse, J.; Lapp, A.; Findenegg, G. H. *J. Phys. Chem. B* **2010**, *114*, 4183–4191.
(24) Jia, H.; Grillo, I.; Titmuss, S. S. *Langmuir* **2010**, *26*, 7482–7488.
(25) Rahme, K.; Oberdisse, J.; Schweins, R.; Gaillard, C.; MArty, J.-D.; Mingotaud, C.; Gauffre, F. *Chem. Phys. Chem.* **2008**, *9*, 2230–2236.
(26) Guerrero-Martínez, A.; González-Gaitano, G.; Viñas, M. H.; Tardajos, G. *J. Phys. Chem. B* **2006**, *110*, 13819.
(27) Pérez-Juste, J.; Pastoriza-Santos, I.; Liz-Marzán, L. M.; Mulvaney, P. *Coord. Chem. Rev.* **2005**, *249*, 1870–1901.
(28) Sethi, M.; Joung, G.; Knecht, M. R. *Langmuir* **2009**, *25*, 317–325.
(29) Jain, P. K.; Lee, K. S.; El-Sayed, I. H.; El-Sayed, M. A. *J. Phys. Chem. B* **2006**, *110*, 7238–7248.
(30) http://www.ill.eu/instruments-support/computing-for-science/cs-software/all-software/sans.
(31) Hubert, F.; Testard, F.; Rizza, G.; Spalla, O. *Langmuir* **2010**, *26*, 6887–6891.
(32) Henkel, A.; Schubert, O.; Plech, A.; Sönnichsen, C. *J. Phys. Chem. C* **2009**, *113*, 10390–10394.
(33) Abécassis, B.; Testard, F.; Spalla, O.; P., B. *Nano Lett.* **2007**, *7*, 1723–1727.
(34) http://www.ncnr.nist.gov/resources/sldcalc.html.
(35) Takahashi, H.; Niidome, Y.; Niidome, T.; Kaneko, K.; Kawasaki, H.; Yamada, S. *Langmuir* **2006**, *22*, 2–5.
(36) Oda, R.; Huc, I.; Schmutz, M.; Canday, S. J.; MacKintosh, F. *Nature* **1999**, *399*, 566.
(37) Menger, F. M.; Keiper, J. S. *Angew. Chem., Int. Ed.* **2000**, *39*, 1907.
(38) Spalla, O.; Lyonnard, S.; Testard, F. *J. Appl. Crystallogr.* **2003**, *36*, 338–347.
(39) Aswal, V. K.; Goyal, P. S.; De, S.; Bhattacharya, S.; Amenitsch, H.; Bernstorff, S. *Chem. Phys. Let* **2000**, *329*, 336–340.